ChemComm
Chemical Communications

Accepted Manuscript

This article can be cited before page numbers have been issued, to do this please use: M. Wang, W. Wan, J. Sun and Y. Liu, *Chem. Commun.*, 2025, DOI: 10.1039/D5CC03014E.

ROYAL SOCIETY OF CHEMISTRY

rsc.li/chemcomm

ChemComm

View Article Online
DOI: 10.1039/D5CC03014E

COMMUNICATION

A Rapid Covalent Tracer to Image Aggresome in Stressed Live Cells

Mengdie Wang[a,b], Wang Wan[a,b], Jialu Sun[a], Yu Liu*[a,b]

Received 00th January 20xx,
Accepted 00th January 20xx

DOI: 10.1039/x0xx00000x

Commercial PROTEOSTAT aggresome detection kit is not compatile with live-cell applications. Here, we report a rapid covalent fluorescent tracer to visualize aggresomes in stressed live cells without cell fixation.

Well-defined 3-dimensional conformation of proteins is essential to acquire their proper physiological functions. The fidelity of protein folding is governed by proteostasis network in cells, which regulates the integrity of proteome from protein expression to degradation[1]. Proteostasis, however, tends to be disrupted by either endogenous or external stressors, leading to aberrant protein misfolding and aggregation. Proteome aggregation underlies the etiology of numerous protein conformational diseases, particularly for neurodegenerative diseases. Intracellular proteome aggregation (i.e. aggresomes) and extracellular amyloid deposition (i.e. amyloid plaques) are common pathological hallmarks for these diseases[2, 3].

Much light has been shed on the detection of protein aggregation by fluorescent sensors. Towards extracellular amyloid deposition, amyloid proteins were visualized by various types of sensors, including derivatives of BODIPYs[4, 5], curcumins[6], aggregation induced emission (AIE) probes[7, 8], metal coordinates[9, 10], fluorescent protein fluorophores[11], etc. In cellular milieu, the only commercially available PROTEOSTAT aggresome detection kit requires cell permeabilization and fixation prior to imaging aggresomes that consist of misassembled intracellular aggregated proteome[12]. Given cellular complexity, fluorescent tracers to detect aggresomes in live stressed cells are limited. [13-15]. (Fig. 1a).

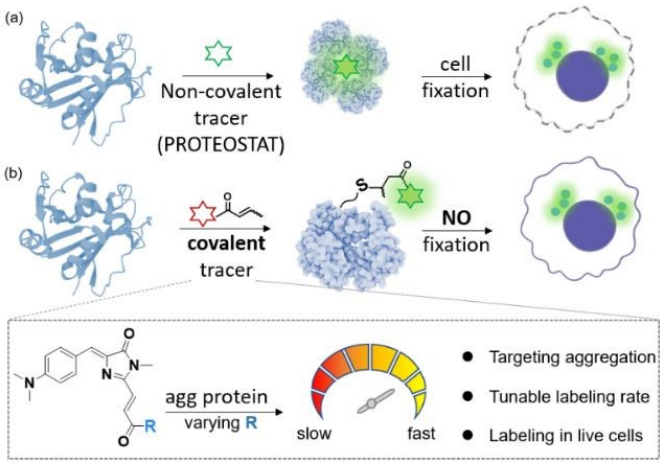

Fig. 1 Fluorescent tracers to detect cellular aggresomes in cells. (a) Non-covalent PROTEOSTAT kit requires cell fixation. (b)This work reported a rapid covalent chemical probe to track proteome aggregation in live cells *via* Michael addition with tuneable labelling kinetics.

The abovementioned protein aggregation sensors are designed based on non-covalent binding mechanism to sense the low-polarity and high-viscosity microenvironments inside protein aggregates. On the other hand, covalent tracers of misfolded and aggregated proteome are developed by taking advantage of exposed and activated nucleophiles upon protein aggregation[16]. Hong and Ohe et al. groups developed fluorescent covalent tracers to label exposed thiol groups during unfolded protein responses[17-19]. Though these covalent tracers of unfolded proteome offer stable fluorescent signal for imaging applications, covalent tracers for cellular aggresomes with rapid labelling kinetics has not yet been reported.

Herein, we introduced a Michael addition based covalent fluorescent tracer to rapidly label and stably image cellular aggresomes in live stressed cells (Fig. 1b). The rapid covalent

[a] *State Key Laboratory of Medical Proteomics, National Chromatographic R. & A. Center, Dalian Institute of Chemical Physics, Chinese Academy of Sciences, Dalian 116023, China.*
[b] *University of Chinese Academy of Sciences, Beijing 100049, China.*
† Electronic Supplementary Information (ESI) available: [details of any supplementary information available should be included here]. See DOI: 10.1039/x0xx00000x

View Article Online
DOI: 10.1039/D5CC07014B

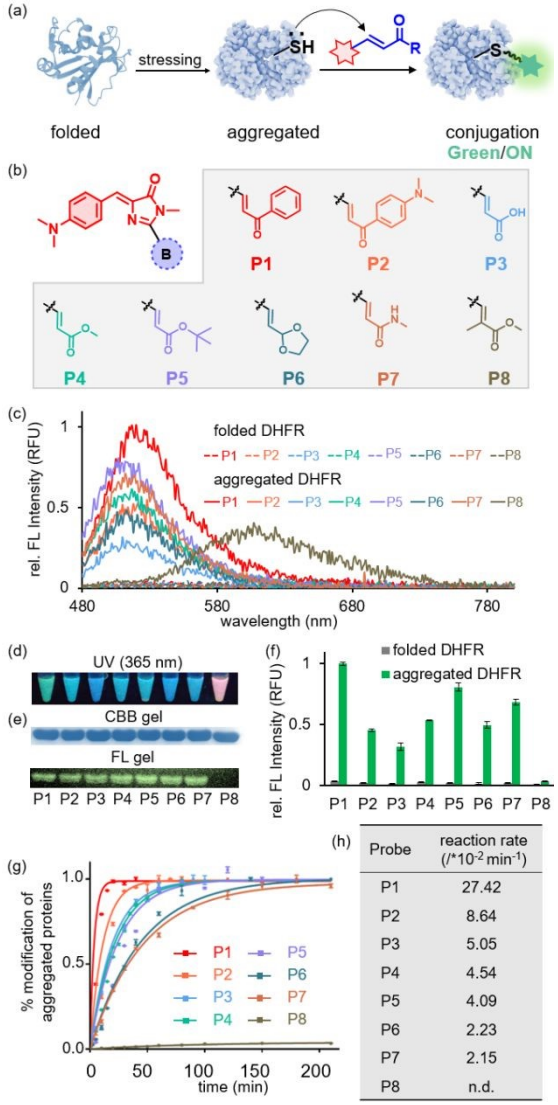

(h)

Probe	reaction rate (/*10^{-2} min^{-1})
P1	27.42
P2	8.64
P3	5.05
P4	4.54
P5	4.09
P6	2.23
P7	2.15
P8	n.d.

Fig. 2 Tuning the labelling kinetics of covalent protein aggregation sensors by modulating the reactivity of Michael acceptor. (a) Mechanism-of-action to detect aggregated proteins by fluorescent covalent sensor. (b) Structure modulation to regulate reactivity of Michael acceptors. (c) The change of emission spectra of P1-P8 upon DHFR aggregation. (d) Photograph of aggregated DHFR incubated with P1-P8. P1-P7 but not P8 color-switched from red to cyan upon heat-induced DHFR aggregation. (e) Electrophoresis gel confirmed covalent conjugation of probes with aggregated DHFR. (f) Rel. FL maximal emission intensity of P1-P8 in aggregates. (g) The labelling kinetics of P1-P8 with aggregated DHFR. (h) Apparent labelling rates were fitted by pseudo 1st order kinetics.

tracer may become useful to develop covalent proximity induced degradation drugs (ATTEC) to ameliorate proteome stresses. We embarked on designing such probe based on the fluorescent protein chromophore, a core scaffold reported to inherently bind to aggregated proteins (Fig. 2a)[13]. To accelerate the labelling kinetics, we rationally tuned the chemical reactivity of the Michael acceptors, resulting P1 to P8 probes (Fig. 2b). As expected, all probes remained fluorescently dark with folded proteins (Fig. 2c. dash lines) but turned on fluorescence upon binding and reacting with aggregated proteins (Fig. 2c, solid lines, Fig. S3). Notably, P8 with steric hindrance showed exclusively red fluorescence with emission maximum at 605 nm, well aligned with the parent FP chromophore in viscous solvent (S7), indicating negligible covalent reactivity of P8 towards aggregated proteins due to steric issue. In contrast, P1 to P7 all shifted their fluorescent emission from the red region to cyan/green region (λ_{em} from 500 nm to 530 nm), suggesting that the conjugation breaks upon Michael addition to aggregated proteins (Fig. 2c, 2d). It was noteworthy that extremely strong electron withdrawing moieties may intensively quenched fluorescence after conjugation (Fig. S9-S10). The covalency upon conjugating to aggregated proteins was eventually evidenced by fluorescent SDS-page gel (Fig. 2e).

Next, we asked whether these Michael acceptors of different electron densities can enhance the labelling kinetics, resulting in a rapid covalent tracer for protein aggregates. We took advantage of green fluorescence emission to monitor covalent conjugation reaction between probes and protein aggregates (Fig. 2f). To compare the reactivity of these probes in protein aggregates, the labelling kinetics was quantified (WT-DHFR: 100 μM; probes: 10 μM; Fig. 2e). The apparent reaction rates of Michael addition were obtained by fitting against pseudo first order kinetics, showing that chemical modulation of carbonyl substitution effectively tuned the labelling kinetics (Fig. 2h). Specifically, the aryl ketones (P1-P2) were more rapid in labelling aggregated protein compared to α, β-unsaturated carboxylic ester/acid (P3-P7). As expected, P8 of steric hindrance showed no covalent reactivity. Among all probes, P1 offered the fastest labelling kinetics with half-life ($t_{1/2}$) at 2.5 min. By tuning the structures of Michael acceptors, we successfully accelerated the labelling kinetics from 0.036 s^{-1} for P7 up to 0.457 s^{-1} for P1. However, the fact that P1 with an electron-rich Michael acceptor offers the fastest labelling kinetics is contradictory to our expectation, possibly because the additional benzene ring (P1 and P2) may contribute to better binding to aggregated proteins (i.e. faster k_{on}).

We further investigated the labelling mechanism of P1, the fastest probe shown in Fig.2. First, we demonstrated that the origin of green fluorescence was caused by protein aggregation. By fractionation experiment, the fluorescence signal was nearly all from the insoluble fraction, but not from the soluble fraction. The Coomassie bright blue (CBB), fluorescence gels and photograph under 365 nm UV-light together echoed this conclusion (Fig. 3b). These results confirmed that P1 fully converted to green fluorescence upon conjugating to aggregated proteins. Next, we ensured the labelling and the consequent color-shifting from red to green was caused by conjugating to a nucleophile *via* nucleophilic 1,4-addition on P1. We selected protected cysteine and ethylamine to mimic cysteine and lysine nucleophilic residues in aggregated proteins, respectively. The P1 probe effectively reacted with model substrates, and the corresponding adducts were verified

View Article Online
DOI: 10.1039/D5CC04145B

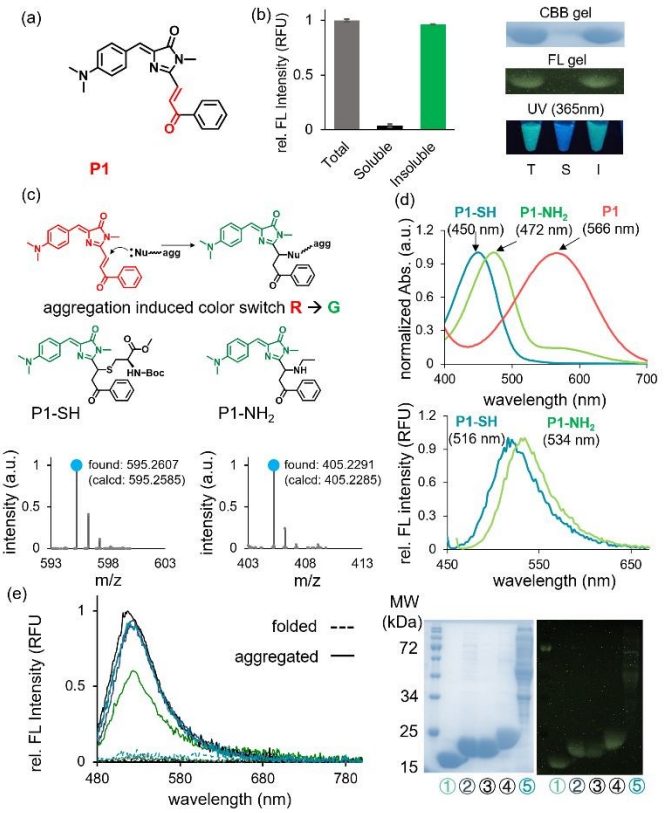

Fig. 3 P1 turned on green fluorescence upon protein aggregation. (a) The structure of P1 probe, the most rapid tracer for covalent labelling of aggregated proteins. (b) Fractionation experiment indicated the fluorescence emission of P1 mainly from conjugating to insoluble aggregates. T: total fraction, S: soluble fraction, I: insoluble fraction. (c) The color of P1 was switched from red to green via Michael addition with nucleophiles. High-resolution mass spectrometry verified the expected Michael addition products. (d) UV-vis and fluorescence emission spectra P1 after conjugating to nucleophilic cysteine and lysine. (e) The fluorescence emission spectra of P1 with folded and aggregated proteins. Fluorescent electrophoresis gel indicated P1 covalently conjugated to proteins.

via high resolution mass spectrometry (Fig. 3c). Similar to the scenario in protein aggregates (Fig. 2c), we observed hypsochromic shift of both absorption and fluorescence emission (red to green) as well (Fig. 3d) in viscous glycerol, well aligned with the one observed in protein aggregates. This observation indicated that fluorescence shift to green color was indeed caused by Michael addition to nucleophiles inside aggregates. Moving forward to aggregated protein scenario, P1 predominantly conjugated with the thiol group of cysteine residues instead of other nucleophilic residues (Fig. S4).

We further validated the generality of P1 probe in covalent labelling toward different types of aggregated proteins. Upon aggregating different recombinant proteins (50 μM) or lysate proteome (1mg·mL^{-1}), P1's green fluorescence gradually enhanced as the temperatures increased after Michael addition to protein aggregates (Fig. 3e). The fluorescence electrophoresis gel also confirmed general covalent conjugation of P1 with these aggregates. Furthermore, we also exemplified P1 to measure the thermodynamic stabilities of these proteins in the thermal shift assay enabled by P1' green fluorescence (Fig. S4-S5).

Finally, we demonstrated that P1 served as a covalent tracer to selectively visualize aggresomes in stressed live cells without previously unwanted fixation protocol. According to abovementioned fluorescence switch properties in buffer, the P1 lit up weak red fluorescence emission upon non-covalently binding with misfolded proteins at the initial acuate stress phase, but further switched to green color upon conjugating to insoluble aggregates accumulated in cellular aggresomes (Fig. 4a). To show such property of P1, cellular proteome aggregation was induced by MG132 to inhibit proper proteosome function, leading to the formation of aggresomes. Upon short-term acuate stress by MG132 for 5h, weakly diffuse red fluorescence signal was observed in cytosol. Severe proteome aggregation in cell was observed after prolonged treatment of MG132 for 24 h. Meanwhile, the punctate aggresome structures with intense green fluorescence were observed exclusively in 488 nm channel (Fig. 4b). Such transformation in fluorescence color echoed the in vitro experimental results using recombinant proteins (Fig. 3).

To further demonstrate its general applicability, P1 probe was also applied to detecting aggresomes in different cell lines including liver cell (AML-12) from mus musculus, or renal epithelial cell (HEK293T), hepatic cancer cell (HepG2), and breast cancer cell (MDA-MB-231) from homo sapiens. As expected, P1 emitted bright green fluorescence upon labelling aggresomes after stressing the cells with MG132 for 24h (Fig. 4c). Besides MG132, other cellular stressors were also tested to demonstrate P1's general applicability in staining aggresomes, including 17AAG (heat-shock protein inhibitor), bortezomib (proteosome inhibitor), chloroquine (inhibitor of lysosome) and cycloheximide (disturb protein synthesis in ribosome) (Fig. 4d). We observed different morphologies of cellular aggresomes under these stressing conditions.

In summary, we developed a rapid covalent tracer to label aggregated proteins *via* Michael addition. The reaction rate was rationally tuned by chemical modifications, yielding up to 10-fold kinetic acceleration. The optimized P1 probe was used to monitor protein aggregation and rapidly label cellular aggresomes in multiple cell lines and stressed conditions. It is not always beneficial to improve labeling kinetics by enhancing electron withdrawing capacity to the extreme but sacrificing selectivity. Balancing the rapid labeling and satisfactory cellular selectivity is a dilemma to be chemically fine-tuned. Our rapid aggresome covalent tracer outperformed the commercial PROTEOSTAT kit with better live cell compatibility without fixation.

M. Wang performed data curation, formal analysis, methodology, software, investigation, visualization W. Wan

performed supervision, resource, validation, funding acquisition writing–original draft, J. Sun performed resource, validation, Y. Liu performed conceptualization, funding acquisition project administration, writing–review & editing.

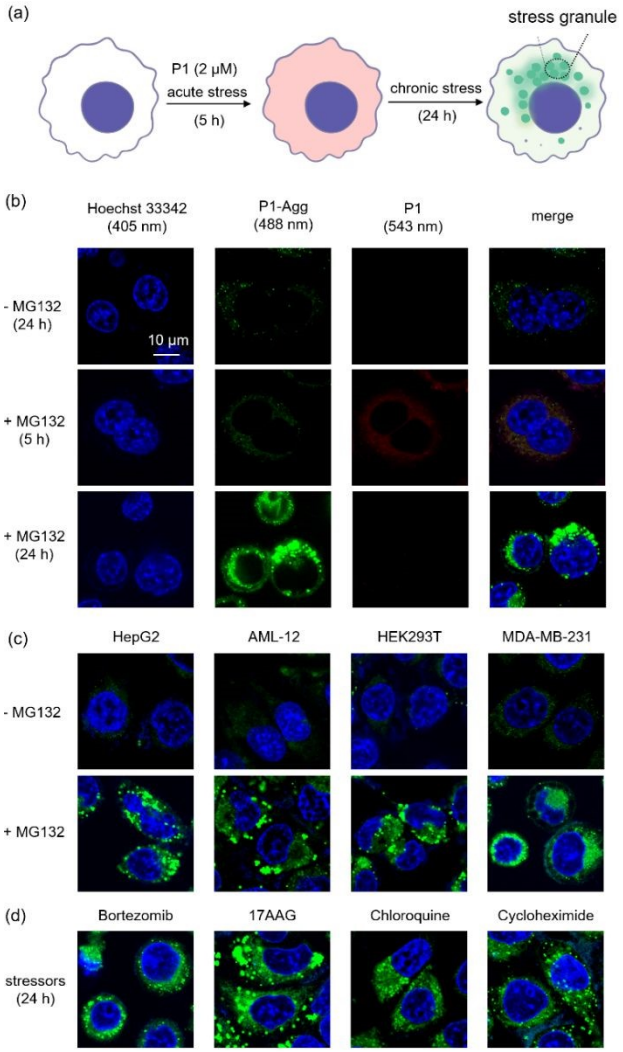

Fig. 4 Imaging cellular aggresomes by P1. (a) Experimental scheme of P1 to detect labelling aggregated proteome in cellular milieu without fixation. (b) Proteome aggregation was induced by MG132 in HEK293T cell for different durations. 5 h caused acuate stress and initial proteome misfolding. 24 h caused prolonged stress and intense insoluble aggregates accumulated in aggresomes. P1 detected aggresomes in different cell lines (c) and under different cellular stressors (d).

This work was supported, in part, by funds from the National Natural Science Foundation of China (22222410, 22374148), Dalian Science and Technology Innovation Fund (2023JJ12WZ037), International Partnership Program of Chinese Academy of Sciences (028GJHZ2023079FN), Innovation Program of Science and Research from the DICP, CAS (DICP I202458).

Conflicts of interest

There are no conflicts to declare.

View Article Online
DOI: 10.1039/D5CC03014E

Data availability

The data supporting this article have been included as part of the SI. Supplementary information: Supplementary figures, Experimental Procedures, Synthesis and NMR spectra.

Notes and references

1. M. S. Hipp, P. Kasturi, F. U. Hartl, *Nat. Rev. Mol. Cell. Biol.* **2019,** *20*, 421-435.
2. W. E. Balch, R. I. Morimoto, A. Dillin, J. W.Kelly, *Science* **2008,** *319*, 916-9.
3. F. Chiti, C. M. Dobson, *Annu. Rev. Biochem.* **2017,** *86*, 27-68.
4. P. Verwilst, H. R. Kim, J. Seo, N. W. Sohn, S. Y. Cha, Y. Kim, S. Maeng, J. W. Shin, J. H. Kwak, C. Kang, J. S. Kim, *J. Am. Chem. Soc.* **2017,** *139*, 13393-13403.
5. B. Shen, K. H. Jung, S. Ye, C. A. Hoelzel, C. H. Wolstenholme, H. Huang, Y. Liu, X. Zhang, *Aggregate*, **2023**, *4*, e301.
6. X. Zhang, Y. Tian, C. Zhang, X. Tian, A. W. Ross, R. D. Moir, H. Sun, R. E. Tanzi, A. Moore, C. Ran, *Proc. Natl. Acad. Sci. U. S. A.* **2015,** *112*, 9734-9.
7. W. Fu, C. Yan, Z. Guo, J. Zhang, H. Zhang, H. Tian, W. H. Zhu, *J. Am. Chem. Soc.* **2019,** *141*, 3171-3177.
8. Y. Hong, L. Meng, S. Chen, C. W. Leung, L. T. Da, M. Faisal, D. A. Silva, J. Liu, J. W. Lam, X. Huang, B. Z. Tang, *J. Am. Chem. Soc.* **2012,** *134*, 1680-9.
9. L. Ge, Y. Tian, *Anal. Chem.* **2019**, *91*, 3294–3301.
10. B. Jiang, A. Aliyan, N. P. Cook, A. Augustine, G. Bhak, R. Maldonado, A. D. S. McWilliams, E. M. Flores, N. Mendez, M. Shahnawaz, F. J. Godoy, J. Montenegro, I. Moreno-Gonzalez, A. A. Mart, *J. Am. Chem. Soc.* **2019**, *141*, 15605–15610.
11. H. Leng, Y. Wang, J. Wang, H. Sun, A. Sun, M. Pistolozzi, L. Zhang, J. Yan, *Anal. Chem.* **2022**, *94*, 1999–2006 .
12. S. Navarro, S. Ventura, *Biotechnol. J.* **2014**, *9*, 1259-1266.
13. W. Wan, W. Jin, Y. Huang, Q. Xia, Y. Bai, H. Lyu, D. Liu, X. Dong, W. Li, Y. Liu, *Anal. Chem.* **2021,** *93*, 1717-1724.
14. Y. Huang, M. Chang, X. Gao, J. Fang, W. Ding, J. Liu, B. Shen, X. Zhang, *ACS Cent. Sci.* **2024***, 10,* 842-851.
15. B. Shen, L. Liu, Y. Huang, J. Wu, H. Feng, Y. Liu, H. Huang, X. Zhang, *Aggregate* **2024,** *5*, e421.
16. W. Wan, Y. Huang,; Q. Xia,; Y. Bai, Y. Chen, W. Jin, M. Wang, D. Shen,; H. Lyu, Y. Tang, X. Dong, Z. Gao, Q. Zhao, L. Zhang, Y. Liu, *Angew. Chem. Int. Ed.* **2021,** *60*, 11335-11343.
17. Mu, H.; Miki, K.; Kubo, T.; Otsuka, K.; Ohe, K., *Chem. Commun.* **2021,** *57*, 1818-1821.
18. Owyong, T. C.; Subedi, P.; Deng, J.; Hinde, E.; Paxman, J. J.; White, J. M.; Chen, W.; Heras, B.; Wong, W. W. H.; Hong, Y., A *Angew. Chem. Int. Ed.* **2020,** *59*, 10129-10135.
19. Sabouri, S.; Liu, M.; Zhang, S.; Yao, B.; Soleimaninejad, H.; Baxter, A. A.; Armendariz-Vidales, G.; Subedi, P.; Duan, C.; Lou, X.; Hogan, C. F.; Heras, B.; Poon, I. K. H.; Hong, Y., *Adv. Healthc. Mater.* **2021,** *10*, e2101300.

View Article Online
DOI: 10.1039/D5CC03014E

Data availability

The data supporting this article have been included as part of the SI. Supplementary information: Supplementary figures, Experimental Procedures, Synthesis and NMR spectra.